AIP Advances

Correlating electron trapping and structural defects in Al_2O_3 thin films deposited by plasma enhanced atomic layer deposition

Cite as: AIP Advances **10**, 125017 (2020); https://doi.org/10.1063/5.0023735
Submitted: 31 July 2020 . Accepted: 20 November 2020 . Published Online: 11 December 2020

Emanuela Schilirò, Patrick Fiorenza, Corrado Bongiorno, Corrado Spinella, Salvatore Di Franco, Giuseppe Greco, Raffaella Lo Nigro, and Fabrizio Roccaforte

COLLECTIONS

Paper published as part of the special topic on Chemical Physics, Energy, Fluids and Plasmas, Materials Science and Mathematical Physics

ARTICLES YOU MAY BE INTERESTED IN

Temperature-dependent electroluminescence study on 265-nm AlGaN-based deep-ultraviolet light-emitting diodes grown on AlN substrates
AIP Advances **10**, 125014 (2020); https://doi.org/10.1063/5.0024179

GaN ultraviolet photodetector with petal-like β-Ga_2O_3 microcrystalline layer
AIP Advances **10**, 125107 (2020); https://doi.org/10.1063/5.0028550

Recent advances in Re-based double perovskites: Synthesis, structural characterization, physical properties, advanced applications, and theoretical studies
AIP Advances **10**, 120701 (2020); https://doi.org/10.1063/5.0031196

© 2020 Author(s).

Correlating electron trapping and structural defects in Al_2O_3 thin films deposited by plasma enhanced atomic layer deposition

Cite as: AIP Advances 10, 125017 (2020); doi: 10.1063/5.0023735
Submitted: 31 July 2020 • Accepted: 20 November 2020 •
Published Online: 11 December 2020

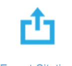

Emanuela Schilirò, Patrick Fiorenza,[a] Corrado Bongiorno, Corrado Spinella, Salvatore Di Franco, Giuseppe Greco, Raffaella Lo Nigro, and Fabrizio Roccaforte

AFFILIATIONS

Consiglio Nazionale delle Ricerche, Istituto per la Microelettronica e Microsistemi (CNR–IMM), Strada VIII, 5 Zona Industriale, 95121 Catania, Italy

[a]Author to whom correspondence should be addressed: patrick.fiorenza@imm.cnr.it

ABSTRACT

In this article, electron trapping in aluminum oxide (Al_2O_3) thin films grown by plasma enhanced atomic layer deposition on AlGaN/GaN heterostructures has been studied and a correlation with the presence of oxygen defects in the film has been provided. Capacitance–voltage measurements revealed the occurrence of a negative charge trapping effect upon bias stress, able to fill an amount of charge traps in the bulk Al_2O_3 in the order of 5×10^{12} cm^{-2}. A structural analysis based on electron energy-loss spectroscopy demonstrated the presence of low-coordinated Al cations in the Al_2O_3 film, which is an indication of oxygen vacancies, and can explain the electrical behavior of the film. These charge trapping effects were used for achieving thermally stable (up to 100 °C) enhancement mode operation in AlGaN/GaN transistors, by controlling the two-dimensional electron gas depletion.

© 2020 Author(s). All article content, except where otherwise noted, is licensed under a Creative Commons Attribution (CC BY) license (http://creativecommons.org/licenses/by/4.0/). https://doi.org/10.1063/5.0023735

INTRODUCTION

Aluminum oxide (Al_2O_3) is an attractive material for a variety of applications in electronic devices.[1] As an example, thin Al_2O_3 layers can be used as a gate insulator to reduce the leakage current in gallium nitride (GaN) high electron mobility transistors (HEMTs) or as a passivation layer to reduce the current collapse phenomena in these devices.[2,3] The great interest toward Al_2O_3 in the GaN technology arises from the excellent physical properties of this insulator, i.e., high dielectric constant κ (~9), high critical electric field (10 MV/cm), large bandgap (~8.9), and favorable band alignment with GaN.[4]

In this context, atomic layer deposition (ALD) is the most widely used technique today to deposit Al_2O_3 thin films on GaN. In fact, ALD is a self-limited growth mechanism, enabling an accurate control of thickness and interface abruptness, and a uniform coverage at low deposition temperatures, i.e., compatible with the GaN thermal stability range and typical device processing.

In general, the quality of amorphous thin films grown by ALD can be extremely variable.[5] In particular, theoretical calculations show that Al_2O_3 layers are characterized by the presence of native defects[6–8] that can also influence their electrical behavior (i.e., leakage current) by introducing electronic levels in the dielectric bandgap.[9,10]

In the last decade, the vast majority of the literature on GaN-based devices focused on the electrical behavior of thermal ALD Al_2O_3 films.[2–4,11–13] Despite in some cases charge trapping phenomena have been observed, which lead to an instability of the Al_2O_3/AlGaN device characteristics,[11,13] a clear correlation of these effects with the structural quality of the film has not been reported.

In this context, plasma enhanced atomic layer deposition (PE-ALD) is a promising alternative to the standard thermal ALD approach, possessing the advantage of higher growth rate and film density and low deposition temperature.[14,15] However, the origin of charge trapping at interface states and bulk oxide traps in PE-ALD Al_2O_3 films on GaN-based heterostructures remains under

© Author(s) 2020

discussion,[16,17] thus hindering the full technological exploitation of these films.

In this paper, the electron trapping phenomena in Al_2O_3 thin films deposited by plasma enhanced atomic layer deposition on AlGaN/GaN heterostructures have been investigated and correlated with the interface and bulk structural quality of the film. In particular, the correlation of capacitance measurements upon stress and structural analyses allowed us to attribute the observed electron trapping to the presence of low-coordinated Al cations, i.e., oxygen vacancies in the Al_2O_3 film. A practical implication of this physical effect on the insulated gate AlGaN/GaN HEMT technology has been discussed, opening the possibility to fabricate thermally stable enhancement mode transistors.

EXPERIMENTAL

Al_2O_3 films have been deposited by Plasma Enhanced ALD (PE-ALD) onto AlGaN/GaN heterostructures grown on Si(111) substrates. Prior to the Al_2O_3 deposition, the AlGaN surface has been treated by a sequential cleaning process using piranha (H_2O_2:H_2SO_4 = 1:5) and diluted hydrofluoric acid (H_2O:HF = 10:1) solutions, for 10 min and 5 min, respectively, in order to remove the carbon contamination and native oxide.[18] These chemical treatments, before the deposition process, were selected among different possibilities, which were explored in earlier research and whose effects on the electrical properties were evaluated.[19] The Al_2O_3 deposition has been carried out on a PE-ALD LL reactor from SENTECH Instruments GmbH, using trimethyl-aluminum (TMA) and O_2-plasma as aluminum and oxygen sources, respectively. The O_2-plasma has been generated by a capacitively coupled plasma (CCP) source, through a 13.56 MHz RF-generator with a power of 200 W. For the plasma run, a 100 sccm O_2 flow was released to the plasma source. Nitrogen (N_2) gas, with a flow rate of 40 sccm, has been used as a carrier for the TMA precursor. During the ALD cycle, pulse periods of 60 ms and 1 s for TMA and O_2-plasma, respectively, have been coupled with the purging pulse of N_2 gas for 2 s. The deposition process has been carried out at 250 °C, with a chamber pressure of 20 Pa. According to the nominal growth rate of 1.2 Å/cycle, the number of cycles was chosen to be 250 in order to obtain an Al_2O_3 film thickness of about 30 nm.

Circular Al_2O_3/AlGaN/GaN metal–insulator–semiconductor (MIS) capacitors were fabricated to monitor the electrical quality of the bulk oxide and of the interface by capacitance–voltage (C–V) measurements under different bias stress conditions. In these control devices, the Ohmic contact was formed by an annealed Ti/Al/Ni/Au multilayer,[20] while the gate contact consisted of a Ni/Au bilayer.

Morphological, structural, and chemical analyses of the deposited Al_2O_3 films were carried out employing a variety of techniques on blanket al_2O_3/AlGaN/GaN samples. In particular, atomic force microscopy (AFM) was carried out to investigate the surface morphology of the films, using a Veeco Dimension 3100 AFM with a NanoScope V controller. High-resolution transmission electron microscopy (HR-TEM) on cross-section samples enabled us to evaluate the film thickness as well as microstructural properties of the Al_2O_3/AlGaN interface. The chemical nature of the Al_2O_3 thin films was investigated by Electron Energy-Loss Spectroscopy (EELS) in the scanning transmission electron microscopy (STEM) mode with a nanometer electron probe. Both kinds of analyses were carried out using a Field Emission Gun-TEM JEOL 2010F microscope.

Finally, Al_2O_3/AlGaN/GaN metal–insulator–semiconductor high electron mobility transistors (MISHEMTs) have been fabricated and characterized by current–voltage (I–V) measurements, monitoring the stability of the transfer characteristics at high temperatures (up to 100 °C). The C–V and I–V measurements on capacitors and transistors were carried out using a Microtech Cascade probe station equipped with a Keysight B1505 parameter analyzer.

RESULTS AND DISCUSSION

The growth of the Al_2O_3 insulating layer on AlGaN/GaN heterostructures has been obtained by the PE-ALD procedure described in detail elsewhere.[19] The role of surface preparation before deposition has been fully exploited, and the effects on the formation of interface defects have already been discussed in previously reported papers.[17–19] Here, the dielectric properties and charge trapping phenomena of Al_2O_3 layers, grown by the PE-ALD optimized procedure,[18,19] have been investigated on Al_2O_3/AlGaN/GaN MIS capacitors, by the C–V measurements, as reported in Fig. 1(a). These measurements have been carried out by sweeping the gate bias from negative toward positive values and backward. Different C–V curves have been sequentially collected by increasing the final gate bias value from 0 V to +15 V on "fresh" (non-stressed) MIS capacitors, and the hysteresis between the forward and backward C–V curves has been determined for each stress condition. In particular, these measurements allowed us to discriminate among the different trapping contributions at the Al_2O_3/AlGaN and AlGaN/GaN interfaces. It should be underlined that the sweeping rate did not affect the value of the hysteresis. The reported C–V curves have been acquired at 0.05 V/s, and each point has been averaged with four measurements. The first C–V measurement [the blue curve in Fig. 1(a)], collected from V_G = −10 V to 0 V and backward, shows no hysteresis. The depletion of the two-dimensional electron gas (2DEG)[21] at the AlGaN/GaN interface is clearly visible with a "pinch-off" of the curves at V_{PO} = −7.5 V. The absence of hysteresis demonstrates that no charge trapping occurs by stressing the MIS capacitor in the negative gate bias range, i.e., at the AlGaN/GaN interface where the 2DEG is located.

Furthermore, C–V curves have been collected by increasing the final positive gate bias stress up to +10 and +15 V [red and black curves in Fig. 1(a)]. Summarizing, the gate stress is applied by extending the V_G bias toward larger positive values. Hence, initially, all the C–V measurements have been carried out at the gate bias ranging from −10 V to 0 V and backward, and then, the final bias value has been progressively increased up to +15 V. Under these conditions, the C–V curves first rise at the "flat band voltage" V_{FB} and then exhibit a second step due to the accumulation of electrons in the AlGaN layer at the Al_2O_3 interface.

The C–V curves exhibit two capacitance saturation levels that correspond to the capacitance of the Al_2O_3 layer (at a high positive gate bias) and to the series capacitance of the Al_2O_3 and AlGaN layer (in the V_G range of −5 V/+5 V). Hence, from the accumulation capacitance, the relative permittivity of the Al_2O_3 layer has been determined to be $\kappa_{Al_2O_3} = 8.4$, which is close to the theoretical Al_2O_3 bulk value (≈9), thus demonstrating the good dielectric quality of deposited films.

© Author(s) 2020

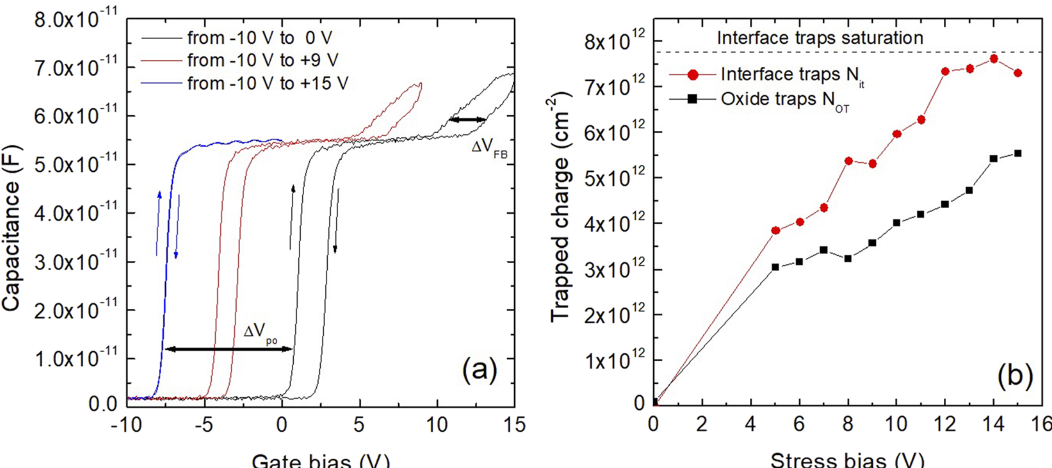

FIG. 1. (a) C–V curves collected on a MIS capacitor sweeping the gate bias from depletion-to-accumulation and backward, by increasing the value of the final gate bias. (b) Total amount of the Al_2O_3/AlGaN interface trapped charge and bulk oxide (Al_2O_3) trapped charge as a function of the positive gate bias stress. The values have been extracted from the C–V curves from the shifts ΔV_{FB} and ΔV_{PO}.

It is interesting to note that the hysteresis of the C–V curves is always observed under positive bias stress conditions, such as close to the pinch-off V_{PO} and to the flat band voltage V_{FB}. These hystereses can be associated with different charge trapping effects occurring in the MIS system.

To quantify these effects, the flat band voltage and pinch-off voltage shifts (ΔV_{FB} and ΔV_{PO}) have been monitored as a function of the positive gate bias stress. In particular, these shifts are associated with the charging of the Al_2O_3/AlGaN interface states (ΔV_{FB}) and of the traps in the bulk Al_2O_3 (ΔV_{PO}).[22] In fact, to provide a quantitative description of the observed charge trapping effects, the following assumptions are needed: (i) the insulator bulk traps are located at the Al_2O_3/AlGaN interface, as often described in the text books,[23] and are responsible for the shift of V_{PO} (ΔV_{PO}) in the C–V curves and (ii) the interface traps at the Al_2O_3/AlGaN interface are completely de-trapped under the application of negative V_G values.

Following the planar capacitor approximation, the total amount of charge trapped at the Al_2O_3/AlGaN interface (N_{it}) can be obtained by

$$N_{it} = \frac{\Delta V_{FB} C_{\mathrm{Al_2O_3}}}{q}, \quad (1)$$

where $C_{\mathrm{Al_2O_3}}$ is the insulator layer capacitance in accumulation and q is the electron charge.

Based on these assumptions, the capacitance plateaux C_{PO} observed close to $V_G = 0$ V are the series of the insulator ($C_{\mathrm{Al_2O_3}}$) and AlGaN layer (C_{AlGaN}) capacitances,

$$C_{PO} = \left(\frac{1}{C_{\mathrm{Al_2O_3}}} + \frac{1}{C_{\mathrm{AlGaN}}}\right)^{-1}, \quad (2)$$

and are related to the V_{PO} shift (ΔV_{PO}) through the following equation [Eq. (3)]:

$$C_{PO} = \left(\frac{1}{C_{\mathrm{Al_2O_3}}} + \frac{1}{C_{\mathrm{AlGaN}}}\right)^{-1} = \frac{\Delta Q}{\Delta V} \equiv \frac{qN_{OT}}{\Delta V_{PO}}, \quad (3)$$

which has been used to calculate the total amount of trapped charges in the Al_2O_3 film (N_{OT}),

$$N_{OT} = \frac{\Delta V_{PO}\left(\frac{t_{\mathrm{Al_2O_3}}}{\kappa_{\mathrm{Al_2O_3}}\varepsilon_0} + \frac{t_{\mathrm{AlGaN}}}{\kappa_{\mathrm{AlGaN}}\varepsilon_0}\right)^{-1}}{q}, \quad (4)$$

where $t_{\mathrm{Al_2O_3}}$ and t_{AlGaN} are the Al_2O_3 and AlGaN layer thicknesses, while $\kappa_{\mathrm{Al_2O_3}}$ and κ_{AlGaN} are the Al_2O_3 and AlGaN relative permittivities.

Figure 1(b) reports the total amount of the trapped charges at the Al_2O_3/AlGaN interface (N_{it}) and in the bulk Al_2O_3 (N_{OT}) as a function of the positive gate bias stress. The values have been extracted from the C/V curves from the shifts ΔV_{FB} and ΔV_{PO}, using Eqs. (1) and (4), respectively.

As can be seen, the value of N_{it} increases with the increase in the final positive bias stress value, until a saturation is observed at high stress bias, corresponding to a maximum of the trapped charge, $N_{it} = 7 \times 10^{12}$ cm^{-2}. In fact, by increasing the positive bias stress, in the MIS capacitor, on the AlGaN/GaN heterostructure, electrons are spilled-over from the 2DEG and reach the Al_2O_3/AlGaN interface, where they can fill the available free traps until reaching saturation. Once the gate bias is swept backward, the Al_2O_3/AlGaN interface states are fully discharged.

On the other hand, the total amount of trapped charges in the bulk Al_2O_3 does not show such a saturation with the increase in the bias stress [Fig. 1(b)]. The occurrence of a positive ΔV_{PO} shift in the C–V curves is associated with the presence of slow traps in Al_2O_3, which retains the negative charge even after strong negative backward gate biasing. Hence, the positive shift occurs from the initial value (non-stressed MIS capacitor) and the ΔV_{PO} in Eq. (2) is calculated from that initial V_{PO} value [see Fig. 1(a)]. In this case,

© Author(s) 2020

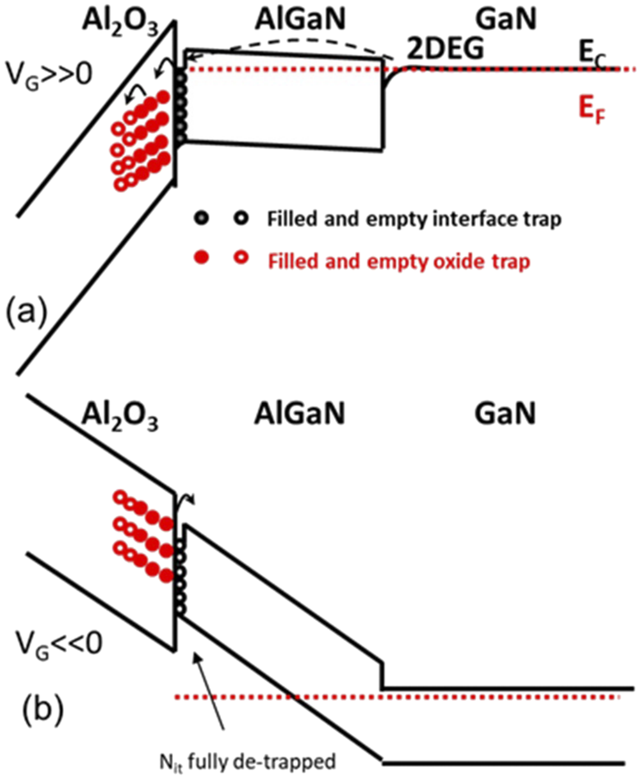

FIG. 2. Schematic energy band diagram of the Al_2O_3/AlGaN/GaN system at different gate bias regimes: (a) $V_G \gg 0$ V, filling the interface and oxide traps with electrons, and (b) $V_G \ll 0$ V, the discharging process of the interface traps and oxide traps.

the maximum of the ΔV_{PO} shift measured after a +15 V stress corresponds to a maximum of $N_{OT} = 5 \times 10^{12}$ cm^{-2}.

The charge trapping/detrapping phenomena occurring in our system are graphically reported in Fig. 2, which shows a schematic band diagram of the Al_2O_3/AlGaN/GaN MIS system.

In particular, when the MIS capacitor is in accumulation ($V_G \gg 0$), the electrons at the Al_2O_3/AlGaN interface can also fill the oxide traps inside the insulator layer (N_{OT}). Once the capacitor is biased in the opposite direction ($V_G \ll 0$), the interface traps are discharged, but the oxide traps retain their charged state. In fact, electrons in bulk oxide traps located near the oxide/nitride interfaces can be retained during reverse bias sweeps due to their long detrapping time even at high temperatures.[17]

The charge trapping phenomena observed in the C/V measurements have been correlated with the morphological and structural properties of the Al_2O_3 films.

The surface morphology of the deposited Al_2O_3 layers has been monitored by using an AFM [Fig. 3(a)] and is characterized by the presence of nanometric rounded grains. The root mean square roughness (RMS) of the film is 0.52 nm, i.e., only slightly higher compared to that of the AlGaN substrate (RMS = 0.32 nm). This latter indicates that the conformal coverage of the AlGaN surface has been achieved.

Then, TEM analysis has been carried out to assess the structural properties of the deposited Al_2O_3 layer and to image its interface with the AlGaN substrate. In particular, the high resolution cross-sectional image (HR-TEM), shown in Fig. 3(b), revealed the formation of an amorphous and uniform layer of Al_2O_3 having a thickness of about 30 nm, with an abrupt Al_2O_3/AlGaN interface and no evidence of an interfacial layer.[24] The good interface quality demonstrates the effectiveness of the surface treatment adopted prior to the PE-ALD and the absence of damage due to the remote plasma.

Further information on the microstructure of the Al_2O_3 film has been gained by the STEM–EELS technique. In particular, Energy Loss Near-Edge Structure (ELNES) investigation has been performed on the sample, focusing on the Al L_{2-3}-edge whose shape is related to Al coordination.[25] In order to have a proper interpretation of the data, the Al L_{2-3}-edge acquired on the PE-ALD deposited Al_2O_3 film has been compared to those of the tabulated defect-free crystalline phases (α-, γ-) Al_2O_3 with known Al-coordination [Fig. 3(c)].[25] The tabulated spectrum of the Al L_{2-3} edge in the α-Al_2O_3 phase [Fig. 3(c), black line], consisting of only octahedrally coordinated Al cations (i.e., six O-coordinated Al), is identified by a high intensity peak centered at 79 eV and a much less intense peak at 80 eV.[25,26] On the other hand, the tabulated Al L_{2-3} edge of the γ-Al_2O_3 phase [Fig. 3(c), red line], consisting of both tetrahedrally (four-coordinated) and octahedrally coordinated Al cations, shows two signals at 78 eV and 79.5 eV, with inverted intensity compared to α-Al_2O_3.[25–27] For both α-phase and γ-phase, the broad peak at about 84 eV is an indication of a medium-range crystalline structure. The experimental spectrum of the Al $L_{2\text{-}3}$ edge obtained on our PE-ALD deposited Al_2O_3 film [Fig. 3(c), green line] shows the absence of the peak at 84 eV due to the lack of the medium range order.[28] Moreover, it exhibits a split broad peak at about 79 eV and 78 eV, having the shape and energy position intermediate between the α- and γ-phase and a second low-energy signal at 76.7 eV. All the features of this edge structure can be related either to the coexistence of four- and six-coordinated aluminum or also to other coordinated aluminum cations (3-, 5-) and, consequently, to the presence of distorted bonds.[25,28–30] The presence of low-coordinated aluminum cations, revealed by our analysis, can be associated with an inherent oxygen deficiency in the Al_2O_3 film. In fact, a*b initio* calculations on low-coordinated aluminum atoms have indicated the presence of transition energy levels in the bandgap of the insulator, which can act as electron traps in the Al_2O_3/AlGaN system.[6]

It is well-known that, besides oxygen vacancies, also other defects, such as residual H and/or C species, could act as charge trapping centers within the dielectric material.[31] For this reason, the quantitative comparison between the experimental density of trapped charges and the amount of oxygen vacancies can be useful. From the ΔV_{PO} of the C–V curves, the amount of trapped charges in the Al_2O_3 of $N_{OT} = 6 \times 10^{12}$ cm^{-2} has been estimated. Assuming the filling of all the bulk traps in the Al_2O_3 layer, their volume concentration (for a thickness of 30 nm) results to be about 2×10^{18} cm^{-3}. In a more realistic scenario, under our bias stress conditions, electron trapping occurs in a limited portion of the insulator, i.e., within about 1 nm from the semiconductor interface, thus resulting in a volume trap charge density of about 6×10^{19} cm^{-3}. Unfortunately, the quantification of the oxygen vacancies in

© Author(s) 2020

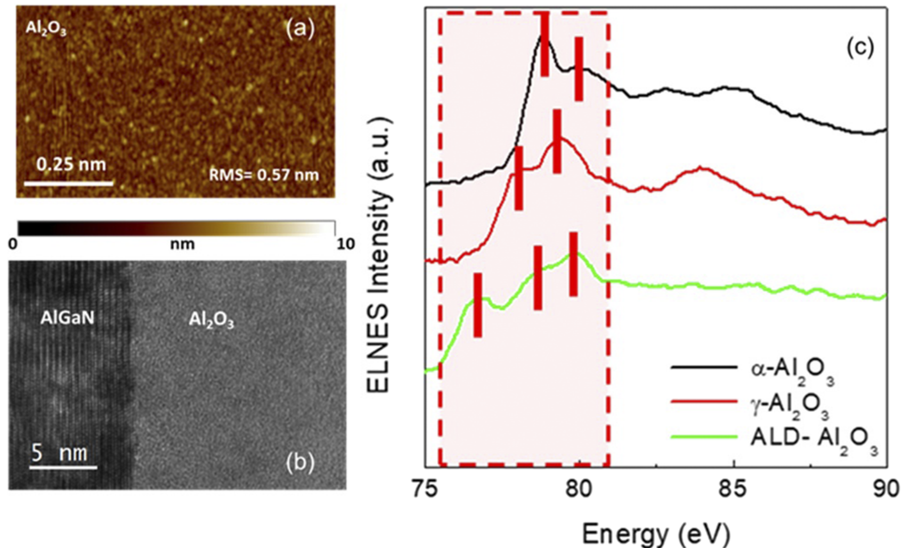

FIG. 3. (a) Morphological map acquired by using an AFM on the 1 × 1 μm^2 areas of the PE-ALD Al_2O_3 thin film. (b) High resolution cross-sectional TEM image of the Al_2O_3/AlGaN interface. (c) Energy loss near-edge structure (ELNES) spectra of the Al $L_{2–3}$-edge for the tabulated α-Al_2O_3 (black line) and γ-Al_2O_3 (red line) and PE-ALD Al_2O_3 thin films (green line).

amorphous Al_2O_3 thin films only by our ELNES spectrum is not straightforward, as it would require standard amorphous Al_2O_3 samples with a known oxygen vacancy content, which are not easily available. In fact, as proposed in the literature for other materials, such a quantification is done mainly by fitting the EELS spectra using theoretical calculations of the amorphous supercell with an appropriate amount of oxygen vacancies.[32,33] The electronic properties of oxygen vacancies in amorphous Al_2O_3 have been discussed in the literature.[9,34] Perevalov *et al.* estimated an oxygen vacancy content for amorphous Al_2O_3 thin films grown by ALD in the order of 7×10^{20} cm^{-3}.[7] Based on the above considerations, since the experimental trapped charge density is lower than the expected oxygen vacancy density, it is plausible to argue that not all these intrinsic defects are electrically active in our system.

Based on the above considerations, since the experimental trapped charge density is lower than the expected oxygen vacancy density, it is plausible to argue that not all these intrinsic defects are electrically active in our system.

Moreover, the presence of negative charges trapped inside the bulk Al_2O_3 gate insulator can induce Coulombic screening of the underlying 2DEG at the AlGaN/GaN interface. Hence, it can be, in principle, used to achieve the enhancement mode operation in AlGaN/GaN HEMT devices, provided that the amount of negative charges trapped in the oxide is of the same order of magnitude of

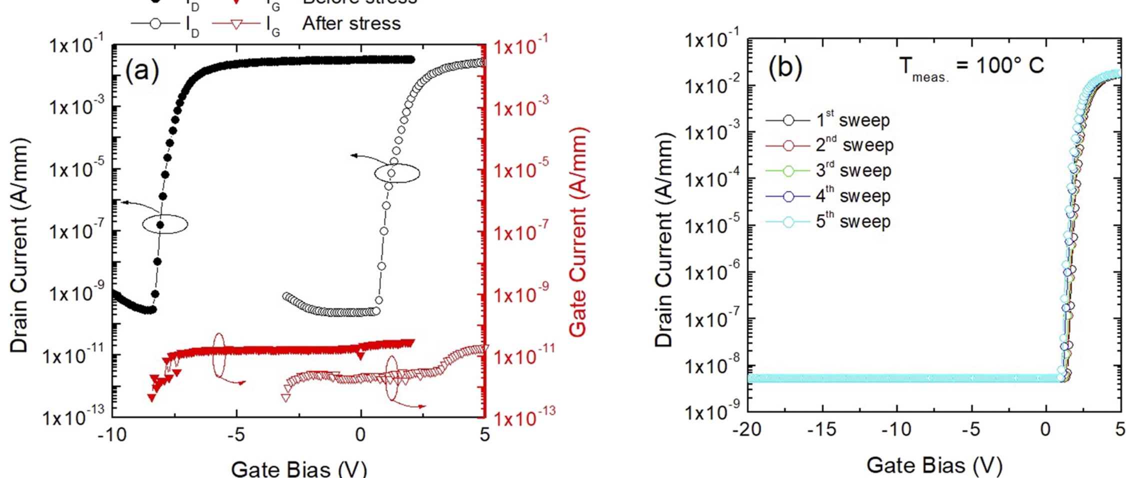

FIG. 4. (a) Transfer I_D–V_G characteristics collected at V_{DS} = 0.1 V for the Al_2O_3/AlGaN/GaN MISHEMT before (solid symbols) and after (open symbols) charge trapping by a positive gate bias at 15 V. The values of the gate current I_G are also shown by red symbols. (b) Series of five I_D–V_G curves (stress at V_G = −20 V) sequentially collected at 100 °C, showing the stability of enhancement mode operation.

© Author(s) 2020

the 2DEG density. The achievement of enhancement mode operation in AlGaN/GaN HEMTs remains one of the most critical aspect in the GaN technology for future power electronics applications.[35]

Figure 4(a) reports the transfer characteristics (I_D–V_G) of the Al_2O_3/AlGaN/GaN MISHEMT before and after a 15 V positive gate bias. As can be seen, after the positive gate bias, the MISHEMT shows an enhancement mode behavior, with a positive pinch-off bias V_{PO} = 1.3 V. At the same time, the transistor still exhibits a low gate leakage current ($I_G \sim 2 \times 10^{-11}$ A/mm at V_G = +5 V). Johnson *et al.*[22] and Hou *et al.*[36] observed an analogous trapping effect in HfO_2 and Al_2O_3 AlGaN/GaN MISHEMTs and attributed it to the presence of a GaON interfacial layer formed during the thermal ALD process. However, in our PE-ALD film, the abrupt interface showed by HR-TEM analysis [Fig. 3(b)] confirms that the electrical behavior is ruled by the presence of structural defects within the Al_2O_3 layer acting as charge traps. Those traps, in turn, seem to have no significant effect on the leakage current.

It is important to point out that the effect of the trapped charges in the Al_2O_3 is stable with the temperature. In fact, Fig. 4(b) reports a sequence of five transfer characteristics of the device collected at 100 °C between V_G = −20 V and +5 V. Evidently, these curves are completely overlapped, thus demonstrating the stability of the film to retain the trapped charge under high temperature operation that requires several days to be relaxed toward the initial condition.

Certainly, the thermal stability of the charge trapping in the bulk traps deserves to be fine controlled in order to achieve fully reliable enhancement mode AlGaN/GaN HEMTs.

CONCLUSIONS

In summary, electron trapping occurring in Al_2O_3 films grown by plasma enhanced atomic layer deposition on AlGaN/GaN heterostructures has been monitored and correlated with the structural properties of the films. In particular, C–V analyses allowed us to monitor the trapping/detrapping effects both in the bulk Al_2O_3 and at the interface, providing an amount of Al_2O_3 bulk traps in the order of $N_{OT} = 5 \times 10^{12}$ cm^{-2}. These defects can be filled with electrons under appropriate positive bias conditions. The ELNES spectra of the aluminum L_{2-3}-edge demonstrated the occurrence of locally low coordinated aluminum cations in Al_2O_3, which are associated with an oxygen deficiency in the film. The local oxygen deficiency can be correlated with the presence of the electron traps in the insulator and can explain the electrical results. This charge trapping phenomenon can be intentionally used to control the depletion of the 2DEG at an AlGaN/GaN interface, obtaining an enhancement mode operation stable up to 100 °C. Hence, the results can be particularly useful for device manufacturers and open new routes for achieving enhancement mode AlGaN/GaN HEMTs.

ACKNOWLEDGMENTS

The authors would like to thank F. Giannazzo (CNR-IMM) for the stimulating scientific discussions. This work was partially funded by the Italian Ministry for Education, University and Research (MIUR) in the framework of the National Project PON EleGaNTe (Electronics on GaN-based Technologies), Grant No. ARS01_01007.

DATA AVAILABILITY

The data that support the findings of this study are available from the corresponding author upon reasonable request.

REFERENCES

[1] G. D. Wilk, R. M. Wallace, and J. M. Anthony, J. Appl. Phys. **89**, 5243–5275 (2001).
[2] F. Roccaforte, P. Fiorenza, G. Greco, M. Vivona, R. Lo Nigro, F. Giannazzo, A. Patti, and M. Saggio, Appl. Surf. Sci. **301**, 9–18 (2014).
[3] T. Hashizume, K. Nishiguchi, S. Kaneki, J. Kuzmik, and Z. Yatabe, Mater. Sci. Semicond. Process. **78**, 85–95 (2018).
[4] F. Roccaforte, P. Fiorenza, R. Lo Nigro, F. Giannazzo, and G. Greco, Riv. Nuovo Cimento **41**, 625–681 (2018).
[5] S.-J. Park, J.-P. Lee, J. S. Jang, H. Rhu, H. Yu, B. Y. You, C. S. Kim, K. J. Kim, Y. J. Cho, S. Baik, and W. Lee, Nanotechnology **24**, 295202 (2013).
[6] M. Choi, A. Janotti, and C. G. Van de Walle, J. Appl. Phys. **113**, 044501 (2013).
[7] T. V. Perevalov, O. E. Tereshenko, V. A. Gritsenko, V. A. Pustovarov, A. P. Yelisseyev, C. Park, J. H. Han, and C. Lee, J. Appl. Phys. **108**, 013501 (2010).
[8] J. Robertson, Solid-State Electron. **49**, 283–293 (2005).
[9] D. Liu, S. J. Clark, and J. Robertson, Appl. Phys. Lett. **96**, 032905 (2010).
[10] J. R. Weber, A. Janotti, and C. G. Van de Walle, J. Appl. Phys. **109**, 033715 (2011).
[11] S. Ganguly, J. Verma, G. Li, T. Zimmermann, H. Xing, and D. Jena, Appl. Phys. Lett. **99**, 193504 (2011).
[12] M. Esposto, S. Krishnamoorthy, D. N. Nath, S. Bajaj, T.-H. Hung, and S. Rajan, Appl. Phys. Lett. **99**, 133503 (2011).
[13] Y. Zhang, M. Sun, S. J. Joglekar, T. Fujishima, and T. Palacios, Appl. Phys. Lett. **103**, 033524 (2013).
[14] H. Kim and I.-K. Oh, Jpn. J. Appl. Phys. **53**, 03DA01 (2014).
[15] D. R. Boris, V. D. Wheeler, N. Nepal, S. B. Qadri, S. G. Walton, and C. R. Eddy, J. Vac. Sci. Technol., A **38**, 040801 (2020).
[16] M. Tapajna, L. Valik, F. Gucmann, D. Gregusova, K. Froehlich, S. Hascık, E. Dobrocka, L. Tothand, B. Pecz, and J. Kuzmık, J. Vac. Sci. Technol., B **35**, 01A107 (2017).
[17] P. Fiorenza, G. Greco, E. Schilirò, F. Iucolano, R. Lo Nigro, and F. Roccaforte, Jpn. J. Appl. Phys. **57**, 050307 (2018).
[18] E. Schilirò, G. Greco, P. Fiorenza, C. Tudisco, G. G. Condorelli, S. Di Franco, F. Roccaforte, and R. Lo Nigro, Phys. Status Solidi C **12**, 980–984 (2015).
[19] R. Lo Nigro, E. Schilirò, G. Greco, P. Fiorenza, and F. Roccaforte, Thin Solid Films **617**, 138 (2016).
[20] G. Greco, F. Iucolano, and F. Roccaforte, Appl. Surf. Sci. **383**, 324–345 (2016).
[21] O. Ambacher, J. Smart, J. R. Shealy, N. G. Weimann, K. Chu, M. Murphy, W. J. Schaff, L. F. Eastman, R. Dimitrov, L. Wittmer, M. Stutzmann, W. Rieger, and J. Hilsenbeck, J. Appl. Phys. **85**, 3222–3233 (1999).
[22] D. W. Johnson, R. T. P. Lee, R. J. W. Hill, M. H. Wong, G. Bersuker, E. L. Piner, P. D. Kirsch, and H. R. Harris, IEEE Trans. Electron Devices **60**, 3197–3203 (2013).
[23] D. K. Schroder, *Semiconductor Material and Device Characterization*, 3rd ed. (Wiley, Hoboken, NJ, 2006).
[24] Q. Wang, X. Cheng, L. Zheng, L. Shen, J. Li, D. Zhang, R. Qian, and Y. Yu, RSC Adv. **7**, 11745–11751 (2017).
[25] D. Bouchet and C. Colliex, Ultramicroscopy **96**, 139–150 (2003).
[26] A. S. Konashuk, A. A. Sokolov, V. E. Drozd, F. Schaefers, and E. O. Filatova, Thin Solid Films **534**, 363–366 (2013).
[27] K. Kimoto, Y. Matsui, T. Nabatame, T. Yasuda, T. Mizoguchi, I. Tanaka, and A. Toriumi, Appl. Phys. Lett. **83**, 4306–4308 (2003).
[28] S. Fritz, A. Seiler, L. Radtke, R. Schneider, M. Weides, G. Weiß, and D. Gerthsen, Sci. Rep. **8**, 7956 (2018).
[29] L. Zeng, D. T. Tran, C.-W. Tai, G. Svensson, and E. Olsson, Sci. Rep. **6**, 29679 (2016).
[30] S. B. Lee, Y.-M. Kim, and H. N. Han, AIP Adv. **5**, 077181 (2015).

© Author(s) 2020

[31] M. Uenuma, K. Takahashi, S. Sonehara, Y. Tominaga, Y. Fujimoto, Y. Ishikawa, and Y. Uraoka, AIP Adv. **8**, 105103 (2018).
[32] K. Dileep, L. S. Panchakarla, K. Balasubramanian, U. V. Waghmare, and R. Datta, J. Appl. Phys. **109**, 063523 (2011).
[33] P. Torruella, C. Coll, G. Martín, L. López-Conesa, M. Vila, C. Díaz-Guerra, M. Varela, M. L. Ruiz-González, J. Piqueras, F. Peiró, and S. Estradé, J. Phys. Chem. C **121**, 24809 (2017).
[34] Z. Guo, F. Ambrosio, and A. Pasquarello, Appl. Phys. Lett. **109**, 062903 (2016).
[35] F. Roccaforte, P. Fiorenza, G. Greco, R. Lo Nigro, F. Giannazzo, F. Iucolano, and M. Saggio, Microelectron. Eng. **187-188**, 66–77 (2018).
[36] B. Hou, X. Ma, J. Zhu, L. Yang, W. Chen, M. Mi, Q. Zhu, L. Chen, R. Zhang, M. Zhang, X. Zhou, and Y. Hao, IEEE Electron Device Lett. **39**, 397–400 (2018).

© Author(s) 2020